Cell Reports
Article

The Mechanisms of Repetitive Spike Generation in an Axonless Retinal Interneuron

Mark S. Cembrowski,[1,*] Stephen M. Logan,[3] Miao Tian,[3] Li Jia,[5] Wei Li,[5] William L. Kath,[1,2] Hermann Riecke,[1] and Joshua H. Singer[3,4]
[1]Department of Engineering Sciences and Applied Mathematics
[2]Department of Neurobiology
Northwestern University, Evanston, IL 60208, USA
[3]Department of Ophthalmology
[4]Department of Physiology
Northwestern University, Chicago, IL 60611, USA
[5]Department of Unit of Retinal Neurophysiology, NEI/NIH, Bethesda, MD 20892, USA
*Correspondence: cembrowski@u.northwestern.edu
DOI 10.1016/j.celrep.2011.12.006

SUMMARY

Several types of retinal interneurons exhibit spikes but lack axons. One such neuron is the AII amacrine cell, in which spikes recorded at the soma exhibit small amplitudes (<10 mV) and broad time courses (>5 ms). Here, we used electrophysiological recordings and computational analysis to examine the mechanisms underlying this atypical spiking. We found that somatic spikes likely represent large, brief action potential-like events initiated in a single, electrotonically distal dendritic compartment. In this same compartment, spiking undergoes slow modulation, likely by an M-type K conductance. The structural correlate of this compartment is a thin neurite that extends from the primary dendritic tree: local application of TTX to this neurite, or excision of it, eliminates spiking. Thus, the physiology of the axonless AII is much more complex than would be anticipated from morphological descriptions and somatic recordings; in particular, the AII possesses a single dendritic structure that controls its firing pattern.

INTRODUCTION

In the mammalian retina, the AII amacrine cell distributes rod-driven synaptic input from the rod bipolar cell to ON and OFF retinal ganglion cells. Often called the rod amacrine cell (Strettoi et al., 1992), recent studies have demonstrated that the AII functions also in cone-mediated vision (Manookin et al., 2008; Münch et al., 2009). Because it operates during both rod- and cone-mediated vision within most of the parallel pathways that generate retinal output, understanding the AII is critical to comprehending signaling within the inner retina.

The AII is an unconventional neuron: it is axonless and has only a soma and an elaborate dendritic tree (Strettoi et al., 1992; Tsukamoto et al., 2001; Veruki et al., 2010). A theoretical study has suggested that the small size of the AII (<100 μm end-to-end distance) makes it electrotonically compact (Vardi and Smith, 1996). Indeed, more recent experimental evidence demonstrated that the AII's dendrites appear to act as a single processing unit: rod-driven synaptic inputs generate synchronous outputs to the ON and OFF pathways despite the fact that the loci of these outputs are on physically separate portions of the dendritic tree (Murphy and Rieke, 2006, 2008; Strettoi et al., 1992; Tian et al., 2010).

Several features of spiking in AIIs, however, are inconsistent with the AIIs' being electrotonically compact. AIIs spike intrinsically at high rates (up to hundreds of Hz), and somatically recorded spikes are small (<10 mV), broad (>5 ms), and capable of superposition (Boos et al., 1993; Tamalu and Watanabe, 2007; Tian et al., 2010; Veruki and Hartveit, 2002a, 2002b). It is unclear how such atypical spike waveforms could be produced in a compact (i.e., isopotential) neuron, as superposing spikes in somatic recordings typically are associated with spike generation at multiple, electrically independent dendritic locations (Oesch et al., 2005). The suggestion of multiple spike initiation sites in AIIs, however, is inconsistent with the recent observation that Na channel expression in AIIs is concentrated on single dendritic processes (Wu et al., 2011).

Here, we combined electrophysiological recordings with computational analyses to elucidate the unconventional anatomical and electrophysiological characteristics of the AII. We found that the AII membrane is not isopotential, nor do spikes arise from multiple dendritic locations. Rather, spikes appear to originate from a single, electrotonically distal site, indicating that the AII has a dendritic compartment that acts like a conventional axon initial segment. At this location, a slow negative feedback mechanism consistent with an M-type K conductance modulates spiking. Our results clarify and expand previous analyses of the AII (Wu et al., 2011) and elucidate the unexpected electrotonic structure of the most common inhibitory interneuron in the mammalian retina (Jeon et al., 1998; Strettoi and Masland, 1996): spikes in the AII are initiated in a single neurite emanating from its

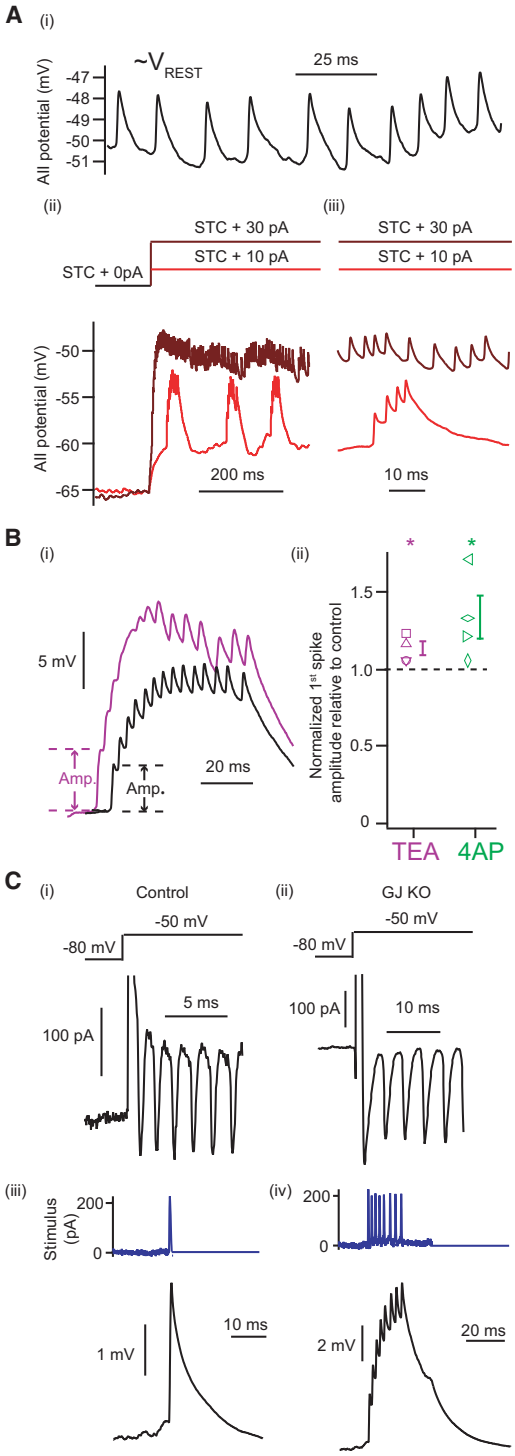

Figure 1. Somatically Recorded Spikes in the AII Appear to Reflect Distal Initiation

(A) (i) Spontaneously occurring spikes at rest exhibited small amplitudes and stereotyped waveforms. (ii) After hyperpolarization of the AII by STC, small current steps induced bursts of superposing spikes. Larger current steps elicited tonic firing. (iii) Expanded view of bursting and tonic spiking.

(B) (i) TEA inhibited recovery and modestly increased the initial spike height. (ii) TEA and 4AP produced significant but small increases in spike height (TEA: 114 ± 4% relative to control; 4AP: 133 ± 14% relative to control; n = 4 cells in each case; $p < 0.05$ in each case; error bars indicate SEM).

(C) In voltage-clamp configuration, a suprathreshold step from −80 to −50 mV evoked regenerative, stereotyped inward events in AIIs from both wild-type (i) and gap junction knockout (ii) mice. In a wild-type AII, injecting a single inward event as depolarizing current in the presence of TTX evoked a waveform similar to a spike in control conditions (iii). Injecting a train of regenerative events in TTX elicited superposing spikes resembling a burst waveform (iv).

elaborate dendritic arbor, and the unconventional pattern of firing observed at the soma is controlled by the interplay of conventional Na and K conductances at this electrotonically distal site.

RESULTS

AIIs Exhibit Small Amplitude Tonic and Burst Firing

We first recorded spiking in AIIs in the light-adapted retina. In accord with previous studies, spikelets exhibited stereotyped waveforms that lacked afterhyperpolarizations (Boos et al., 1993; Tian et al., 2010; Veruki and Hartveit, 2002a, 2002b; Wu et al., 2011; Figure 1Ai). Additionally, when hyperpolarized to threshold (Vthres approximately −60 mV; achieved by injection of hyperpolarizing DC subthreshold current or "STC" of −30 to −80 pA), small depolarizations evoked burst firing (Figure 1Aii,iii). During bursts, high-frequency spikes superposed. When larger current steps were imposed on the STC, bursting behavior was eliminated, and AIIs spiked tonically.

Thus, AIIs can exhibit both tonic and burst firing, and the mode of firing is voltage dependent. This finding provides a useful experimental paradigm to assess the conductances involved in spiking in the AII.

K Conductances Do Not Strongly Limit Spike Height

To begin to understand the electrical organization of the AII, we began by posing a simple question: why are somatically recorded spikes in AIIs small relative to those of classical neurons? Small spikes might reflect a fast K conductance attenuating depolarizations mediated by a voltage-gated Na conductance (Scott et al., 2007). This scheme is plausible, as K currents in AIIs show a prominent A-type component (Boos et al., 1993; Tian et al., 2010). Blocking the A-type K conductance with TEA or 4-AP, however, produced only small increases in the height of the initial spike in a burst (Figure 1B; see Experimental Procedures for why initial spike used).

As an alternative, spikes could be initiated in one or more dendritic compartments isolated electrotonically from the soma by morphological choke points or by leaky dendrites. The small spikes recorded at the soma might therefore represent attenuated versions of larger, dendritically initiated spikes.

Here, we provide experimental evidence for this assertion: in voltage-clamp, a step in somatic holding potential from −80 mV to −50 mV evoked regenerative, TTX-sensitive inward action currents (n = 4, Figure 1Ci). To exclude the possibility that poor voltage control arose from electrical coupling between AIIs, we recorded identical unclamped action currents from AIIs in the Cx36−/− mouse, in which electrical coupling between AIIs is absent (n = 4/4, Figure 1Cii; Deans et al., 2002). We conclude,

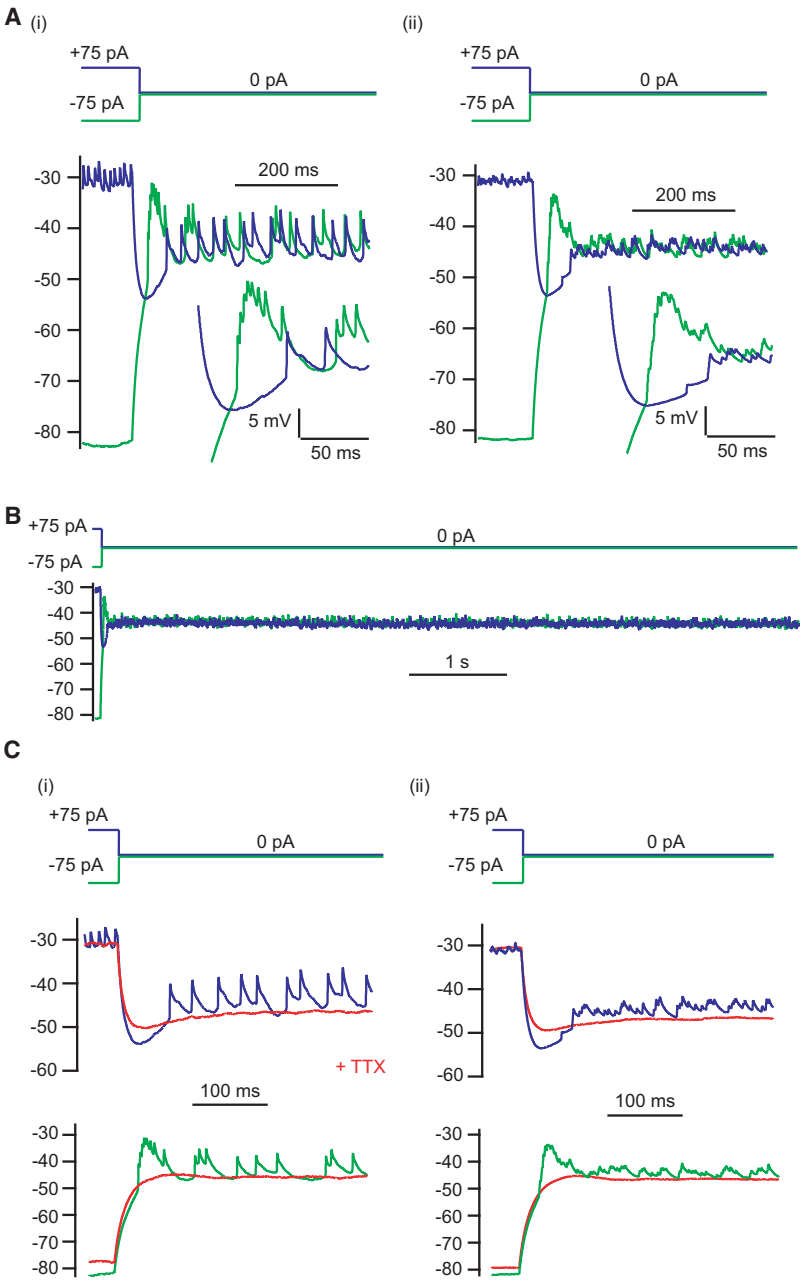

Figure 2. Slow Modulation Is Bidirectional, Exhibits One Timescale, and Is Distal

(A) Repolarization in the AII is illustrated following either a +75 pA (blue) or −75 pA (green) current injection, for a single trial (i) and an average across trials (ii). Respectively, responses exhibited transient after-hyperpolarizations and after-depolarizations with similar time courses.

(B) Responses over a longer time window did not show any further adaptation (averaged response depicted).

(C) TTX (red) strongly reduced transient behavior following current offset in both protocols. Both an individual trial (i) and an averaged response (ii) are shown.

Spiking Is Modulated Bidirectionally on a Single Timescale

Generally, intrinsic bursting requires regenerative spiking modulated by negative feedback from a slower conductance (Izhikevich, 2007). To begin to characterize the slow conductance operating in AIIs, first we assessed the voltage range over which it was active. We considered two possible scenarios. One, the slow conductance might require hyperpolarization to operate, potentially explaining why cells burst following hyperpolarization (Figure 1Aii,iii). Two, the slow conductance might also be active at more depolarized potentials, and therefore modulate spiking bidirectionally; in particular, returns from depolarization should suppress firing owing to the slow adaptation of this conductance.

To differentiate between these two cases, we examined after-potentials at current offset following large hyperpolarizing or depolarizing current injections. In all AIIs tested (n = 6/6), transient bidirectional modulation was observed: rapid superposing bursts of spikes (after-depolarizations) were evoked following returns from hyperpolarization, whereas spiking was transiently suppressed (after-hyperpolarizations) following depolarization (Figure 2Ai, single trial; Figure 2Aii, averaged response). Importantly, these after-depolarizations and after-hyperpolarizations were comparable in duration: this finding suggests that a single conductance could underlie both properties. Finally, their timescales were similar to those of spontaneous, regenerative bursts seen near threshold (Figure 1Aii).

For a subset of cells from the previous protocol (n = 3/6), we looked for additional adaptation on longer timescales by tracking voltage responses for ~7 s after current offset. For all cells examined (three of three), we saw no evidence for additional adaptation (Figure 2B).

then, that the majority of voltage-gated Na channels in the AII must be located at a site (or sites) electrotonically distal to the soma.

To investigate whether these Na currents were the source of spikelets, recorded TTX-sensitive action currents were injected via the recording pipette in the presence of TTX. A single action current waveform elicited a voltage response resembling a spikelet (Figure 1Ciii), and the injection of a train of action currents evoked superposing spikes resembling a burst (Figure 1Civ). These results suggest that the action currents observed in voltage-clamp underlie spiking in current-clamp, and therefore spiking occurs even when somatic voltage is held fixed.

Slow Modulation Occurs Distal to the Soma

Where is the site of the slow conductance relative to the soma? If located electrotonically proximal to the soma (and therefore controlled by somatic voltage), application of TTX should eliminate

spiking but not the underlying slow after-potentials. Alternatively, if the slow conductance is located distally (e.g., close to regenerative conductances), TTX might exert large effects on the after-potentials by blocking the large local voltage spikes driving slow modulation.

We found that blocking Na channels with TTX strongly reduced the transient after-depolarizations and after-hyperpolarizations (example trace, Figure 2Ci; averaged response, Figure 2Cii). This finding supports our assertion that the slow conductance is located distal to the soma and likely found at the spike initiation site(s).

The fact that TTX blocked both after-depolarizations and after-hyperpolarizations is again consistent with both these effects potentially being attributable to a single conductance. However, because these findings provide only indirect support for this assertion, we next sought to directly identify a single conductance responsible for both phenomena.

The Slow Conductance Appears to Be an M-Type K Conductance

The slow conductance modulating bursting in AIIs resembled an M-type K conductance for three reasons. One, it was active near spike threshold and modulated spiking bidirectionally; two, the timescales of afterpotentials were on the order of M-type current kinetics observed in other systems; three, no further adaptation occurred following the afterpotentials, in agreement with the noninactivating nature of M channels (Adams et al., 1982a; Robbins et al., 1992). Therefore, we tested the hypothesis that an M-type K conductance interacts with the Na conductance to generate bursting behavior. We blocked the underlying channels with the M-type K channel antagonist linopirdine dihydrochloride (LP; 30 μM) (Aiken et al., 1995; Schnee and Brown, 1998) and observed the effect on burst duration: if an M-type K conductance is critical for terminating bursts, LP should increase burst duration.

In the presence of LP, the durations of evoked bursts were prolonged (n = 7). In three of seven AIIs, spikes/burst increased and bursting was maintained (control versus LP spikes/burst: 3.9 ± 1.1 versus 15.3 ± 3.0; n = 3; $p < 0.05$; Figures 3A and 3B). In the remaining four of seven AIIs, bursting was abolished altogether, and cells exhibited only tonic spiking following depolarization (Figure 3C). LP did not affect the height of spikes within the bursts, suggesting that it did not block the A-type K conductance to any appreciable extent (Figure S1G available online).

Separately, we investigated how LP affected input resistance and resting membrane potential by injecting current ramps into recorded AIIs. These recordings were done in the presence of TTX to prevent changes in spiking from confounding these measurements. LP depolarized AIIs and increased Rn at potentials depolarized to −55 mV (Figure 3Di). For recordings in which after-hyperpolarizations were evident following current offset (six of ten AIIs), LP either decreased their amplitudes (n = 2/6) or abolished them entirely (n = 4/6) (Figure 3Dii). These results are consistent with LP blocking an M-type K conductance.

Qualitatively identical results were obtained using Ba^{2+} (250 μM) to block M-type K conductances (Adams et al., 1982b; Kotani et al., 2000; Figures S1A–S1C and S1G), as well as with the high-affinity antagonist XE-991 (10 μM) (Wang et al., 1998; Zaczek et al., 1998; Figures S1D–SG). Furthermore, we eliminated contributions to bursting from other, non-M-type K

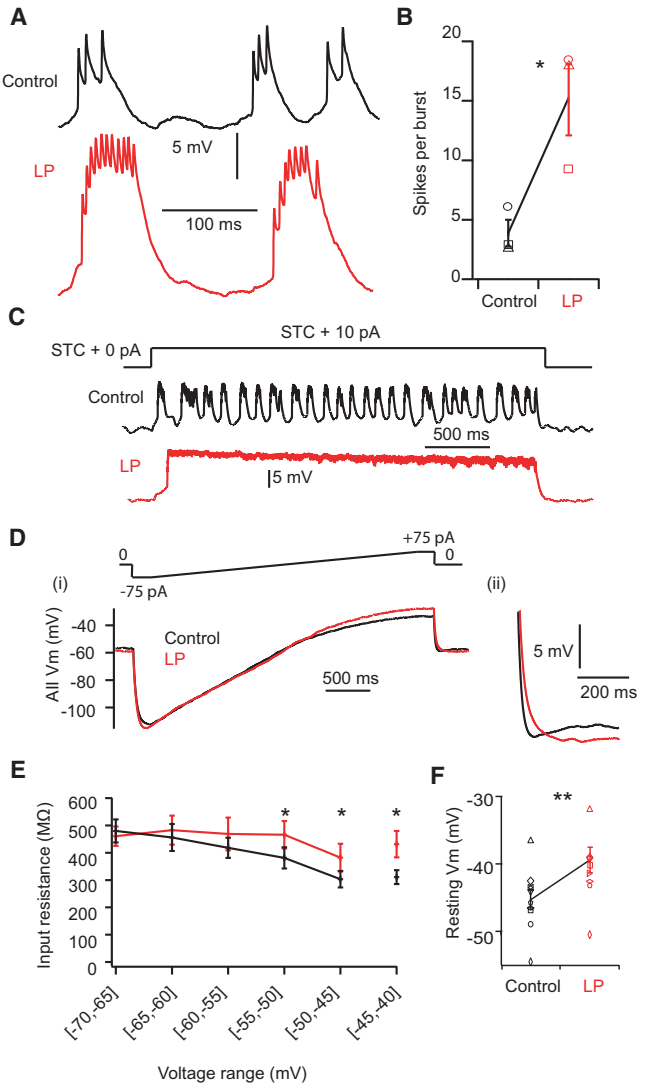

Figure 3. Results from Pharmacological Manipulations Are Consistent with Modulation by an M-Type K Conductance

(A) LP increased spikes/burst in the AII.

(B) Summary data from cells not exhibiting complete loss of burst mode (control versus LP spikes/burst: 3.9 ± 1.1 versus 15.3 ± 3.0; n = 3; $p < 0.05$).

(C) Example trace from an AII where bursting was abolished (n = 4 total).

(D) In the presence of TTX, an AII was ramped (i) from −75 to +75 pA over 2 s in control (black) and after LP was applied (red). Following current offset (ii), the small after-hyperpolarization was eliminated in the presence of LP.

(E) Summary of input resistances, after partitioning the ramp response into 5 mV voltage intervals, in control and LP (see Experimental Procedures; $p > 0.05$ for voltages intervals below −55 mV, and $p < 0.05$ otherwise; only five of ten cells reached voltages of at least −40 mV in both control and LP and the [−45 mV, −40 mV] data point represents data from this subset of cells; n = 10 for all other intervals).

(F) Summary of the change in resting potential following the addition of LP (control: −45.2 ± 1.5 mV, LP: −39.2 ± 2.0 mV; n = 10; $p < 0.01$).

All error bars indicate SEM. See also Figure S1.

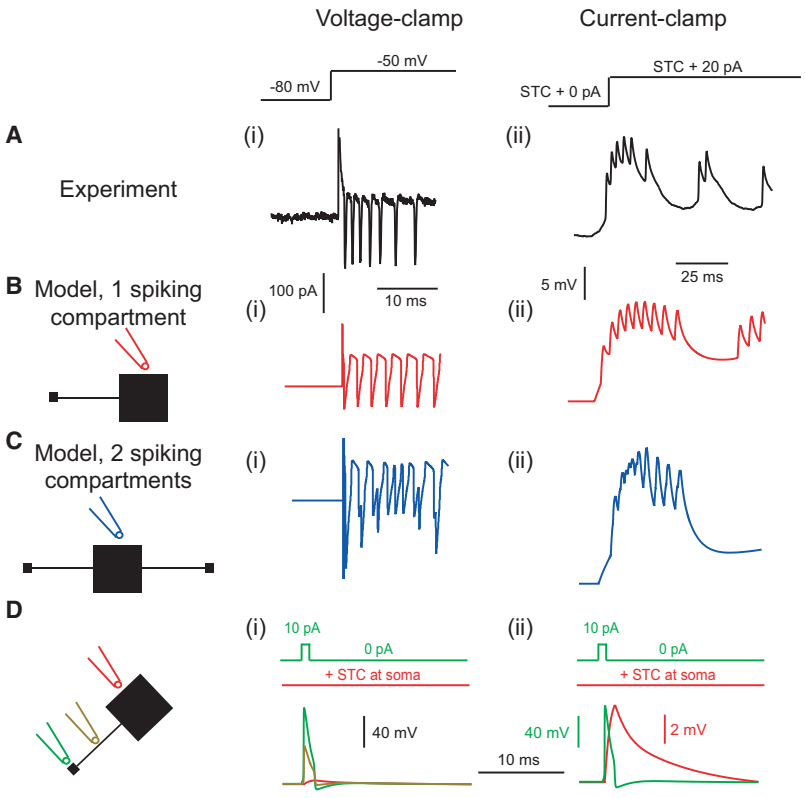

Figure 4. A Computational Model Captures Properties of Experimentally Observed Spiking Only When a Single Initiation Site Is Present

(A) Experimentally recorded action currents (i) and bursts (ii).

(B) A model with a single initiation site (see Table S1) reproduced experimental behavior in both voltage- (i) and current-clamp (ii).

(C) A model with two initiation sites produced simulated somatic recordings which were disorganized and inconsistent with experimental results.

(D) A single dendritic spike was evoked by applying a 1 ms, 10 pA current pulse at the initiation site, which was otherwise kept from firing via STC injection at the soma. The voltages across the AII compartments are shown (i), as well as an expanded view of the somatic response relative to the initiation site response to illustrate the change in time course (ii).

conductances (voltage-gated Ca channels, persistent Na channels, HCN channels, and Ca-gated channels; Figures S1H and S1I). These findings therefore suggest that spiking undergoes slow modulation from an M-type K conductance exclusively.

Spikes Are Initiated in a Single Compartment Only

The previous results illustrate that spikes are generated electrotonically distal to the soma, but do not address the number of independent spike initiation sites. Therefore, we employed a compartmental model of the AII (constrained by our previous experiments; see Experimental Procedures and Table S1) to examine how the activity of one or more distal initiation sites would be reflected in somatic responses. Model AIIs were subjected to the same current injections and voltage steps that were applied experimentally (Figure 4A), and simulated and recorded responses were compared.

Simulated responses from a model with a single initiation site reproduced the features of spiking seen experimentally (Figure 4B): voltage steps evoked repetitive, stereotyped action currents, and current injections elicited bursts of superposing spikes with the interspike interval exhibiting a clear refractory nature. A model with two initiation sites, however, failed to recapitulate the experimental data (Figure 4C). Specifically, action currents and spikes exhibited haphazard superposition and the refractory period between spikes was eliminated. Incorporating additional spiking compartments (>2) caused the model's predictions to deviate further from the experimental responses. Thus, these simulations attest to the existence of a single, distal spike initiation site.

To understand how spikes from a single initiation site transformed and superposed in current-clamp recordings, we tracked the propagation of a single spike across the model AII membrane (Figure 4D). We found that the somatic response was a highly filtered representation of the fast, distally initiated spike: as the spike arrived at the soma its waveform was attenuated and broadened, acting to conceal the initiation site AHP and recovery. As the somatic potential did not reflect the recovery dynamics at the initiation site, rapid distal firing events from a single site could produce superposing waveforms at the soma.

The Model AII Captures and Elucidates Experimental Recordings

Having verified that a simple AII model with one initiation site could capture basic properties of AII spiking, we confirmed the robustness of this model by simulating the experiments of Figures 1–3 and used the model to gain mechanistic insight into these results.

First, we found that the model AII exhibited bursts with superposing spikes near spike threshold, whereas tonic spiking occurred at more elevated potentials (Figure 5A, cf. Figure 1A). Bursting arose from rapid firing being gradually overwhelmed by recruitment of the slow K conductance; tonic firing occurred at more depolarized potentials when the slow K conductance could not suppress spiking completely (Figures S2A–S2D).

Second, simulating the antagonism of K channels recapitulated experimental results (Figure 5B, cf. Figure 1B). A 75% reduction in the A-type K conductance, mimicking application of 2 mM TEA (Tian et al., 2010), produced a small increase in initial spike height. Moreover, this A-type K reduction also produced a perturbed burst waveform similar to that seen in experiments; this somatic response represented the filtered initiation site voltage after recovery was impaired (Figures S2E and S2F). Conversely, reducing or completely eliminating the slow K conductance did not change the initial spike height (cf. Figure S1).

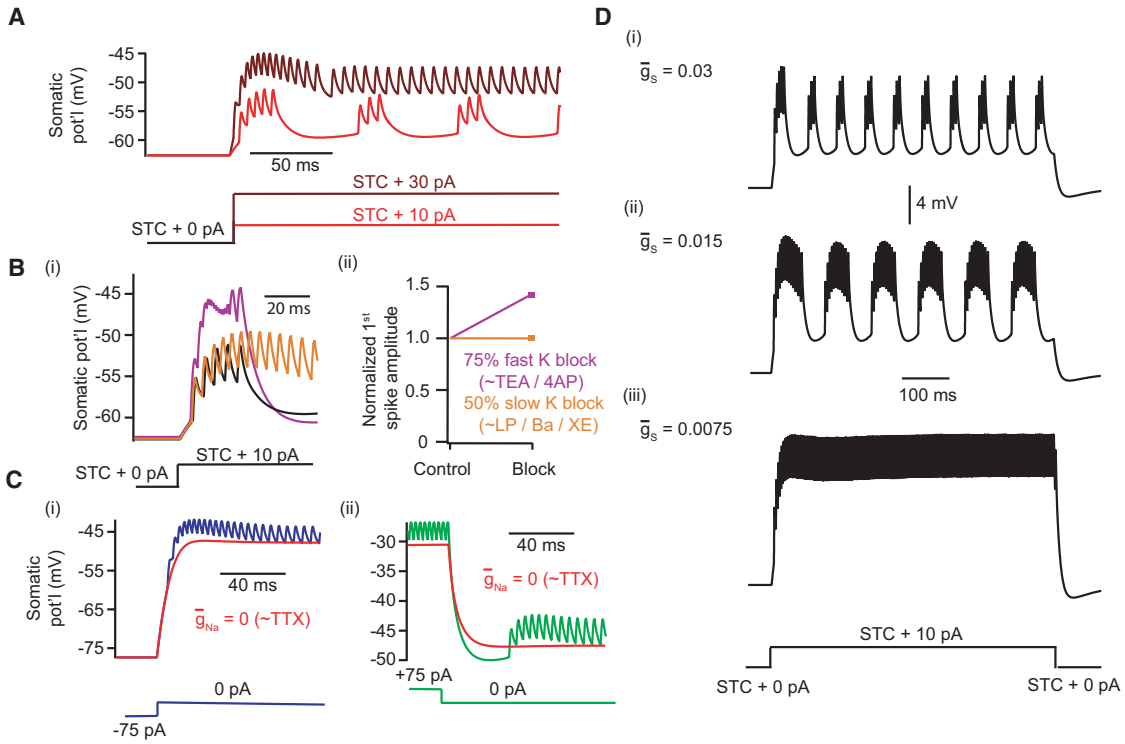

Figure 5. The Single Initiation Site Model Captures Many Features of AII Behavior

(A) Somatic responses to small (10 pA) and large (30 pA) current steps following STC showed bursting and tonic firing, respectively. See also Figures S2A–S2D.

(B) Somatic voltage traces following K channel reduction, simulating the effects of TEA/4AP and LP/Ba/XE application. Results are shown for control (black), for a 75% reduction of fast A-type K density (purple, 143% initial spike height relative to control), and for a 50% reduction of slow K density (gold, 100% initial spike height relative to control). See also Figures S2E and S2F.

(C) Somatic voltages following large depolarizing (i) or hyperpolarizing (ii) current offsets are illustrated. After-hyperpolarizations and after-depolarizations were present and greatly reduced by eliminating Na channels from the model (red).

(D) Reducing the density of slow K prolonged the burst mode in the model AII.

Third, the AII model captured the transient TTX-sensitive after-potentials (Figure 5C, cf. Figure 2), which emerged from the difference in kinetics between fast Na and slow K channels observed upon long depolarizations/hyperpolarizations of the AII. After-depolarizations occurred because the Na conductance activated more quickly than the slow K conductance following return from hyperpolarization; after-hyperpolarizations occurred because the slow K conductance deactivated slowly upon return from depolarization.

Fourth, the model captured LP-, XE-, and Ba-induced prolongation of bursts (Figure 5D, cf. Figure 3; Figure S1). At intermediate reductions in slow K density, bursts were prolonged but still terminated; for larger reductions in density, the burst mode was eliminated altogether and the model AII exhibited only tonic spiking. More in-depth analysis of this transition determined that the model underwent a subcritical Hopf bifurcation as slow K density was increased, and exhibited hysteresis when slow K density was subsequently decreased (data not shown) (Izhikevich, 2007).

Experimental Evidence for a Single, Distal Initiation Site

Our model neuron with a single initiation site reproduced the experimental data well, and we therefore sought to verify the existence of such a site experimentally. We did this in three ways.

One, we applied TTX locally to individual neurites visualized after filling recording AIIs with a fluorescent tracer (see Experimental Procedures). We targeted a single process that appeared to be distinct from the dendritic arbor; in some cases, this neurite could be observed clearly extending away for some distance from its origin on the primary dendrite (Figure 6Ai, arrow; see also Wu et al., 2011). Local application of TTX (50 nM) to the distal termini of these neurites suppressed or completely eliminated spikes recorded at the somata (Figure 6Aiv). In contrast, application of TTX to other portions of the dendritic tree, including compartments as close as 10–20 μm to the distal termini, had noticeably weaker effects (Figures 6Aii–iv). In particular, in every cell tested, the strongest suppression of spiking was observed following application of TTX to the distal terminus. It is notable that in some instances, this terminus was physically well-separated from the remainder of the neuron (e.g., Figure 6Ai), likely minimizing TTX exposure to the vast majority of the AII membrane.

Two, we removed the distal portion of the target neurite to demonstrate that its presence was required for spike initiation: while recording spikes with a somatic recording pipette

containing a fluorescent tracer, the visualized neurite was drawn into a second pipette and pulled away from the cell. After removing the distal portion of this neurite, spiking was completely abolished in the AII (Figure 6Bi; n = 7). Importantly, this occurred despite peak ramp currents typically inducing depolarizations >20 mV above the previous V_{thres} (Figure S3).

This loss of spiking was likely not due to deterioration of cell health. In a subset of cells from the previous protocol (n = 2), prior to removing the putative initiation site, we were able to excise additional neurites without affecting spiking (filled symbols, Figure 6Biii). Moreover, in a separate group of cells (outlined symbols, Figure 6Bii,iii; n = 3), removing noninitiation site neurites did not affect spiking. Thus, the removal of the distal portion of a single and specific neurite was sufficient to eliminate spiking in the AII.

Three, if spiking is indeed initiated at a single site on the AII morphology before propagating passively toward the soma, it would be expected that Na channel expression also would be concentrated at a single site. Therefore, we used immunohistochemistry to examine the localization of Na channels and the Na channel-binding protein ankyrin-G on AIIs: retinae in which AIIs express GFP under the control of the Fbxo32 promoter (Gong et al., 2003; Siegert et al., 2009; Figure 6Ci) were incubated with antibodies against GFP, ankyrin-G, and Na channels (see Experimental Procedures). In tranverse sections, we found that anti-Na channel and anti-ankyrin-G antibody labeling was colocalized and restricted to individual neurites like those studied electrophysiologically (Figure 6Cii). We examined these processes in more detail in retinal whole mounts: GFP-expressing neurites exhibiting ankyrin-G expression clearly extended from the proximal portions of individual AIIs (Figure 6Ciii; note the anti-Na channel antibody was not used in whole-mount experiments because it generated more nonspecific (background) signal than the anti-ankyrin-G antibody). These results are consistent with a recent report (Wu et al., 2011) and bolster our electrophysiological and computational evidence for a single, distal site underlying spiking.

A Morphologically Realistic Model Reproduces Experimental Results

Having described the dendritic compartment constituting the spike initiation site, we thought it important to extend our inquiries beyond a three-compartment model and to verify that a model with a realistic morphology captured the experimental results. An AII was filled and imaged (see Experimental Procedures and Table S2), revealing the presence of a long cable branching asymmetrically from the primary dendrite (Figure 7A; arrow: putative initiation site). A morphologically realistic model based on this imaged AII yielded attenuation between the initiation site and soma similar to that generated by the three-compartment AII (Figures 7B and 7C; cf. Figure 4D). Additionally, the morphologically realistic model generated the dual modes of firing seen experimentally and in the simple model (Figure 7D; cf. Figures 1 and 5A).

Importantly, this detailed model illustrated that the extent of attenuation was very similar at the soma, lobular appendages, and arboreal dendrite (Figure 7C). Therefore, the reduction of the morphologically complex AII into a simple three-compartment model is justified when considering spike dynamics. In addition, this finding suggests that spike heights are similar at the physically separated locations where AIIs contact ON and OFF cone bipolar cells (via electrical and chemical synapses, respectively).

DISCUSSION

Here, we demonstrated that spikelets recorded in the soma of the axonless AII amacrine cell represent large events generated at a single, electrotonically distal initiation site. At this distal dendritic location, a voltage-gated Na conductance appears to be colocalized with a slow M-type K conductance. Spikes generated at this site resemble action potentials that undergo filtering as they propagate to the soma where they are recorded. A morphologically realistic model suggests the waveform of spikes in the complex dendritic arbor is similar to that at the soma. The AII exhibits an unexpected and interesting electrotonic structure: despite its small size, it contains an electronically remote dendritic compartment that, due to the interplay between resident Na and K conductances, modulates the electrical behavior of the neuron as a whole.

Dual Modes of Firing in the AII

Owing to modulation by an M-type K conductance, the AII exhibits two firing modes: bursting near threshold and tonic firing at more depolarized potentials. Na channel-mediated amplification of inputs, then, is likely to vary with the resting potential of the AII, as has been demonstrated previously (Tian et al., 2010).

The resting membrane potential of the AII in vivo is unknown. Reports of AII resting potentials from experiments in vitro vary significantly and do not exhibit a clear dependence on either species or the adaptational state of the retina: −65 mV (dark-adapted mouse, Pang et al., 2004), −59 mV (light-adapted rat, Boos et al., 1993), −50 mV (light-adapted mouse, Tian et al., 2010), −46 mV (dark-adapted mouse, Dunn et al., 2006), −37 mV (dark-adapted mouse, Tamalu and Watanabe, 2007). Although the reason(s) for this variability is (are) unclear, it is notable that these resting potentials span a voltage range in which both modes of firing can occur. Thus, it is reasonable to expect that the AII might exploit both in a physiological setting.

The AII's resting membrane potential appears to depend on the voltage of coupled ON cone bipolar (CBs). It has been shown that application of L-AP4, which hyperpolarizes both rod bipolars (RBs) and ON CBs by agonizing their metabotropic glutamate receptors, also produces large (15–20 mV) hyperpolarizations in AIIs (Tamalu and Watanabe, 2007). We have found similar results when transmission from RBs is blocked (data not shown), suggesting that synaptic activity in gap junction-coupled ON CBs can shape the AII resting potential. This arrangement could provide a means by which activity in ON CBs modulates the excitability of AIIs; in particular, hyperpolarized ON CBs could bias AIIs toward bursting in darkness, whereas depolarized ON CBs might induce tonic spiking in brighter scenes.

Bursts may also act as a mechanism to enhance drive to gap junction-coupled cells. Individual spikes in AIIs are heavily

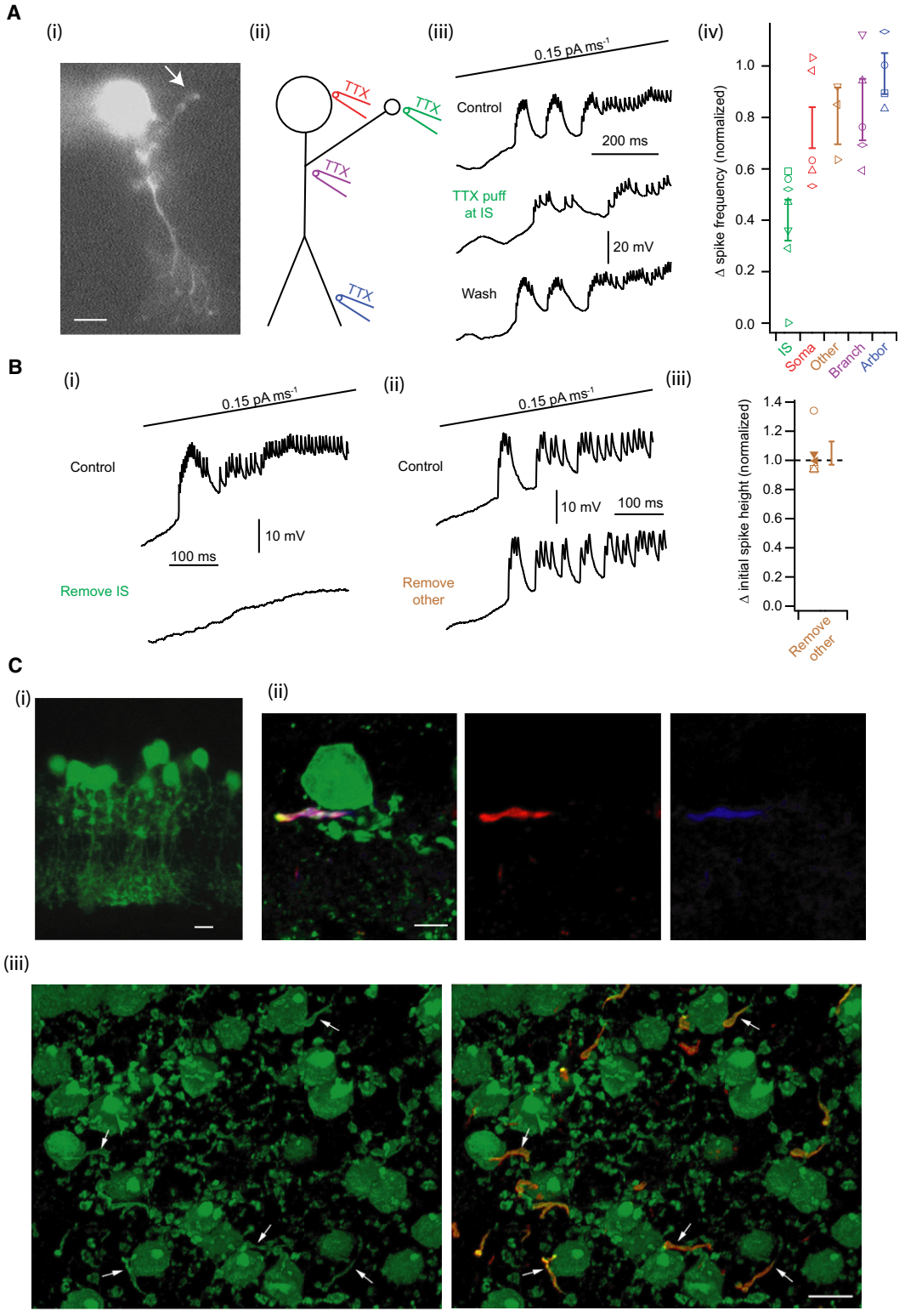

Figure 6. Direct Experimental Evidence for a Single, Distal Initiation Site

(A) TTX application to a visualized putative initiation site (i, scale bar = 5 μm; illustrated schematically in ii) reversibly suppressed spiking during a slow current ramp (iii). (iv) Summary of the reduction in normalized spike frequency following local application of TTX (see Experimental Procedures) (initiation site "IS": 0.40 ± 0.08, n = 7; soma: 0.76 ± 0.12, n = 5; other: 0.80 ± 0.10, n = 3; branch: 0.83 ± 0.11, n = 5; arbor: 0.97 ± 0.08, n = 4; error bars indicate SEM).

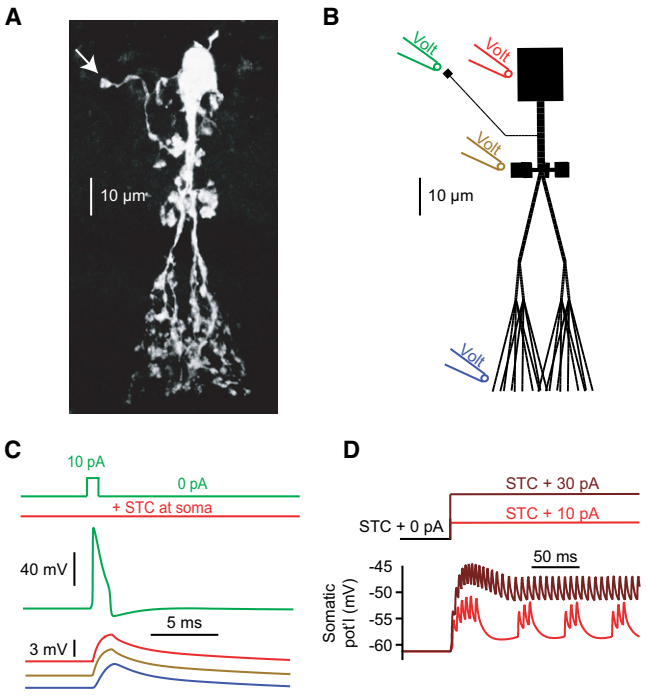

Figure 7. A Morphologically Detailed Model Behaves Similarly to the Reduced Three-Compartment Model and Captures Experimental Responses

(A) A confocal image of an individual AII. A long, unbranched cable with a putative initiation site was present (arrow).

(B) The morphologically detailed model AII (see Table S2), with respective recording locations illustrated.

(C) A single dendritic spike was evoked in the detailed AII by applying a 1 ms, 10 pA current pulse at the initiation site, which was otherwise kept from firing via STC injection at the soma (cf. Figure 4D). The spike attenuated significantly as it propagated toward the primary dendrite. After reaching this neurite, however, voltage responses were similar at the soma, lobular appendages, and distal dendritic arbor (traces offset for clarity).

(D) The detailed morphological model exhibited both burst and tonic firing.

filtered across gap junctions and therefore propagate poorly between coupled cells (Veruki and Hartveit, 2002a, 2002b). Superposing spikes, as typically seen in burst waveforms, may provide a way to circumvent this filtering by producing amplified responses that are relatively broad in time. In this way, the mode of firing (burst versus tonic spiking) may be an important determinant in transmitting Na-mediated events across gap junctions. This could provide a means of modulating the receptive field size of the AII, complementing the plasticity inherent to the AII-AII gap junctions themselves (Bloomfield and Völgyi, 2004; Veruki et al., 2008).

A Single Initiation Site Is Consistent with Published Observations

A recent study of Na channel expression in AIIs indicated that Na channels in these neurons are clustered primarily in a single process (Wu et al., 2011; see also Figure 6). Here, we demonstrate not only that this process functions as a spike initiation site, but also that its electrophysiological characteristics control the surprisingly complex firing patterns observed in the AII.

Our finding that the spike initiation site is electrotonically isolated from the neuron as a whole is consistent with various studies of AII function. Specifically, in studies of AIIs' electrical synapses, passive transmission of spikes between coupled neurons was observed (Veruki and Hartveit, 2002a, 2002b). This result suggests that spikes are not generated near gap junctions, which are found in the distal dendritic arbor (Strettoi et al., 1992; Tsukamoto et al., 2001). In addition, our morphologically realistic model predicts passive propagation of spiking across the arbor (Figure 7C).

Additional evidence that the spike-generating mechanism is isolated comes from the observation that TTX has equivalent effects on the timing of AII output to the ON and OFF pathways (via gap junctions and inhibitory glycinergic synapses, respectively) (Tian et al., 2010). As gap junctions are located primarily on the distal dendrites and glycinergic presynaptic terminals are found in proximal lobular appendages (Habermann et al., 2003; Strettoi et al., 1992; Tsukamoto et al., 2001), it is likely that active spiking does not occur at or between these sites.

Finally, the AII's soma can be excluded as the site of spike initiation, as no Na currents are found in nucleated patches excised from the soma (Tian et al., 2010). Na channels, however, are likely located close to the soma and proximal dendrite (Tamalu and Watanabe, 2007). The identification of a single, thin neurite that branches from the AII's primary dendrite as the spike initiation site (Figures 6A and 7A) fulfills the requirement that Na channels be spatially close to the AII soma while remaining electrotonically isolated from the rest of the cell.

Implications for Circuit Processing

The AII is a multifunctional neuron that plays important roles in both rod- and cone-mediated vision (Deans et al., 2002; Field et al., 2009; Manookin et al., 2008; Münch et al., 2009; Völgyi et al., 2004). How does the unconventional electrotonic structure of the AII contribute to processing within these various pathways? Based on our finding of an isolated functional spiking zone on a distinct AII process, it is natural to ask whether this process has its own dedicated inputs or outputs. Such strategically placed inputs could control the firing of the cell, and with it, modulate the processing of the other inputs that are distributed across the remainder of the dendrite. At the same time, outputs on the specialized process would likely have characteristics that

(B) Following excision of the putative initiation site (i), a ramped AII became quiescent. In a different AII (ii), a putatively nonspiking neurite was removed without eliminating firing. (iii) Summary of the normalized change in initial spike height following removal of nonspiking neurites (postremoval = 105 ± 8% of control, n = 5; $p > 0.05$; error bars indicate SEM). See also Figure S3.

(C) (i) A confocal image of a transverse, in vitro slice preparation of the Fbxo32-GFP retina revealed GFP fluorescence confined largely to neurons with the distinct morphology of AIIs. Scale bar = 5 µm. (ii) In a transverse section of retina, a GFP-expressing AII (green) was labeled with antibodies against ankyrin-G (red) and Na channels (pan-Na; blue). The Na channels and ankyrin-G were colocalized in a single process that appeared to extend from the AII's primary dendrite. Scale bar = 5 µm. (iii) In a retinal whole-mount, GFP-expressing AII somata and dendrites were visualized (green). GFP-positive processes that were clearly connected to AIIs (arrows) expressed ankyrin-G (red). Scale bar = 10 µm.

are quite different from those throughout the remainder of the dendrite as a consequence of direct coupling to spiking.

While such inputs and outputs have not been established functionally, anatomical work using immunohistochemistry (Wu et al., 2011) and EM (Anderson et al., 2011) indicates that they may exist (but see Van Wart et al., 2005, which failed to localize synaptic vesicle markers to Na-channel dense processes resembling these neurites). Moreover, in recordings, weak RB input reliably evoked firing in control conditions but generated almost no somatic response after TTX application (Figure 5 in Tian et al., 2010). This finding is suggestive of some RB inputs being electrotonically close to the spike initiation site, and raises the intriguing possibility that spiking may preferentially amplify scotopic inputs. Thus, an important goal is to determine whether there are indeed functional synaptic contacts that are electrotonically proximal to the AII initiation site, and if so, to what type(s) of cell(s) it establishes connections. This will provide substantial insight into the contributions of the AII to the visual processing performed by the retinal circuitry.

Conclusions

It is interesting to note that, in addition to the AII, two other classes of amacrine cells have been shown to be noncompact. These two cell types exploit different advantages of this electrotonic structure. In the starburst amacrine cell, individual neurites act as independent electrical units to produce direction-selective dendritic calcium signals (Euler et al., 2002). In the A17 amacrine cell, serial dendritic varicosities are separated by thin processes and function in isolation of one another, acting to process signals in parallel while minimizing wiring cost (Grimes et al., 2010). Thus, of the three largest known populations of amacrine cells (Strettoi and Masland, 1996), all have been shown to behave in a noncompact fashion.

EXPERIMENTAL PROCEDURES

Tissue Preparation and Electrophysiological Experimentation

Retinal slices (200 μm thick) were prepared from retinae isolated from adult (P28-56) light-adapted C57BL/6 wild-type and Cx36 knockout (Deans et al., 2001) mice, as described previously (Tian et al., 2010). Cx36 knockout mice exhibited much higher input resistances (R_n = 1.6 ± 0.6 GΩ; n = 6) compared to wild-type mice (R_n ~400–500 MΩ; Figure 3E), consistent with gap junctions being disrupted in Cx36 knockout mice. The Animal Care and Use Committee of Northwestern University approved all procedures involving animal use.

Current- and voltage-clamp recordings were made from AIIs superfused with an artificial CSF at near-physiological temperature (~34°C) as described previously (Tian et al., 2010) (see Extended Experimental Procedures for solution composition). Chemical synaptic transmission was blocked pharmacologically (see Extended Experimental Procedures). Access resistances were typically <25 MΩ; compensation was not used and junction potentials were not corrected.

In experiments where TTX was applied locally, we blocked Na channels by pressure ejection of 50 nM TTX to visualized neurites via a small pipette (tip diameter < < 1 μm; tip resistance ~12 MΩ) filled with HEPES-buffered ACSF (40 mM HEPES substituted for NaH_2CO_3) and positioned near structures visualized by epifluorescent illumination of Alexa tracers included in the somatic recording pipette. TTX-containing solution was ejected by gentle pressure applied by mouth: we found this to be better at generating a spatially restricted bolus of TTX within the slice than the use of a mechanical apparatus like a Picospritzer. We first targeted varicosities distributed asymmetrically around the AII primary dendrite, which often seemed to be coupled to the primary dendrite via an unbranched neurite (e.g., Figure 6Ai, arrow). When these asymmetrical neurites could be visualized clearly, TTX application to them suppressed dramatically or completely reduced the somatically recorded spikes. In some recordings, no asymmetric neurite stood out as a clear candidate initiation site, likely because one was obscured by other structures. When this occurred, multiple compartments were targeted in succession until a TTX-sensitive one was identified. In such instances, only one site exhibited a strong TTX sensitivity; other candidate sites are included in the analysis and denoted as "Other" in Figure 6Aiv. In this figure, spike frequency was calculated as the spike rate averaged over the 300 ms time window following the initial spike (average of 3–4 trials).

To excise the putative initiation site from a spiking neuron, after the target neurite was visualized (as above), the distal terminus was drawn by gentle suction (applied by mouth) into a pipette filled with HEPES-buffered ACSF (as above). Once the distal terminus was within the pipette, the pipette was then gently pulled away from the recorded cell and the process was observed to separate from the recorded cell.

Data analysis was performed using IGOR Pro (Wavemetrics) and Microsoft Excel (Microsoft). Paired, two-tailed t tests were used to compare paired datasets, with significance accepted as $p < 0.05$. Data are presented as mean ± SEM, with some figures also including symbols denoting individual cells.

Analysis of Recordings

Spikes were detected by applying a threshold to the derivative of current-clamp recordings, and bursts were identified as groups of spikes with sequential interspike intervals of <20 ms. As intraburst spiking tended to exhibit interspike intervals ≤8 ms and interburst intervals generally were > = 40 ms (e.g., Figure 1Aii), the choice of a 20 ms window was able to separate periods of bursting from quiescence. The amplitude of individual spikes exhibited some dependence on the timing within a burst; therefore, when examining the effects of K channel antagonists on spike height (Figure 1B; Figure S1), we restricted our analysis to the first spike within a burst. The initial spike height was defined as the maximal difference in voltage in the window of time between the onsets of the first and second spikes in a burst (illustrated on representative bursts in Figure 1Bi).

Computational Model

All numerical simulations were performed with the computational software NEURON (Hines and Carnevale, 1997) using the variable timestep (CVODE) method.

The three-compartment morphology consisted of the following: a large cylinder (the "soma") connecting to a thin cable (the "cable") terminating in a varicosity (the "initiation site"). The large model soma was taken to represent the electrical equivalent of the soma and arboreal dendrite of the AII. The cable and initiation site were taken to represent the long neurite and terminal varicosity branching asymmetrically from the AII primary dendrite, with respective lengths and diameters taken from measurements obtained through confocal imaging (LSM 510; Carl Zeiss) of an individual AII filled with Alexa 594. The morphologies, as depicted in Figure 4, have had the cables and initiation sites enlarged only for purposes of illustration. The cable was taken to be passive, and Hodgkin-Huxley-like active conductances were added to the soma and initiation site. An incompletely inactivating A-type conductance, with parameters constrained by voltage-clamp recordings (Tian et al., 2010), was inserted into both sections. The initiation site contained additional fast Na and slow noninactivating K conductances. For simulations incorporating two spiking compartments, a second identical cable and initiation site were included and connected to the soma. For comprehensive details on simulations using the stylized morphologies, see Extended Experimental Procedures and Table S1.

For simulations of a morphologically realistic AII, we reproduced an AII filled with a fluorescent tracer (see Extended Experimental Procedures and Table S2 for specific measurements). As in the three-compartment model, active conductances were inserted into the initiation site whereas the associated cable was passive. The soma was also taken to be passive, as has been demonstrated experimentally (Tian et al., 2010). A-type K was distributed uniformly across the remaining structures, with the density employed in the three-compartment model. All parameters associated with the active and passive

conductances were identical to those used in the three-compartment model. See Extended Experimental Procedures for details.

Immunohistochemistry

Retinae were isolated from Fbxo32-GFP mice generated by the GENSAT project (Gong et al., 2003; Siegert et al., 2009). Frozen sperm (FVB background) was obtained from the NIH Mutant Mouse Regional Resource Centers (MMRC), and in vitro fertilization of ova from c57bl/6 mice and implantation of fertilized ova into c57bl/6 females was performed by the Transgenic and Targeted Mutagenesis Laboratory at Northwestern University. Mice were bred for > 5 generations into the c57bl/6 background before being used for experiments.

After isolation into oxygenated Ames' medium, retinae were fixed for 15 min in paraformaldehyde (4% in 0.1 M PBS) and then washed extensively in standard solution (0.1 M sodium phosphate buffer plus 0.5% Triton X-100 and 0.1% NaN3 [pH 7.4]) and blocked overnight in standard solution plus 4% donkey serum and Mouse on Mouse (M.O.M) Blocking Reagent (Vector Labs, MKB-2213). Retinae were then incubated with primary antibodies including a chicken antibody against GFP (1:100, Aves Labs, GFP-1020), a mouse antibody against Ankyrin G (1:100, Santa Cruz Biotechnology, sc-12719) and a rabbit antibody against Pan Nav (1:50, Alomone, ASC-003) for 5 days at 4°C. After washing, secondary antibodies (Alexa 488-conjugated donkey anti-chicken, Cy3-conjugated donkey anti-mouse and Cy5-conjugated donkey anti-rabbit antibodies) were applied overnight at 4°C.

Retinae were also embedded in 5% agarose and cut into 150 μm sections on a vibratome and stained with above described primary (overnight at 4°C) and secondary antibodies (1 hr at room temperature).

Images were acquired with a LSM-510 confocal microscope (Zeiss) and processed in Zeiss Zen and Photoshop software.

SUPPLEMENTAL INFORMATION

Supplemental Information includes three figures, two tables, and Extended Experimental Procedures and can be found with this article online at doi:10.1016/j.celrep.2011.12.006.

LICENSING INFORMATION

ACKNOWLEDGMENTS

This work was supported by EY017836 to J.H.S., NIH-CRCNS EY021372 to J.H.S., W.L.K., and H.R., a NSF Graduate Research Fellowship to M.S.C., an unrestricted grant from Research to Prevent Blindness (RPB) to the Department of Ophthalmology at Northwestern, and the NEI intramural research program to W.L. J.H.S. is a RPB Special Scholar for Retinitis Pigmentosa. We are very grateful to Dr. D. Paul for supplying the Cx36 knock-out mice. We thank Dr. T. Jarsky for many helpful discussions, Dr. J. Demb for comments on drafts of the manuscript, and V.J. Dudley for technical assistance.

Received: November 22, 2011
Revised: December 14, 2011
Accepted: December 21, 2011
Published online: February 9, 2012

REFERENCES

Adams, P.R., Brown, D.A., and Constanti, A. (1982a). M-currents and other potassium currents in bullfrog sympathetic neurones. J. Physiol. *330*, 537–572.

Adams, P.R., Brown, D.A., and Constanti, A. (1982b). Pharmacological inhibition of the M-current. J. Physiol. *332*, 223–262.

Aiken, S.P., Lampe, B.J., Murphy, P.A., and Brown, B.S. (1995). Reduction of spike frequency adaptation and blockade of M-current in rat CA1 pyramidal neurones by linopirdine (DuP 996), a neurotransmitter release enhancer. Br. J. Pharmacol. *115*, 1163–1168.

Anderson, J.R., Jones, B.W., Watt, C.B., Shaw, M.V., Yang, J.H., Demill, D., Lauritzen, J.S., Lin, Y., Rapp, K.D., Mastronarde, D., et al. (2011). Exploring the retinal connectome. Mol. Vis. *17*, 355–379.

Bloomfield, S.A., and Völgyi, B. (2004). Function and plasticity of homologous coupling between AII amacrine cells. Vision Res. *44*, 3297–3306.

Boos, R., Schneider, H., and Wässle, H. (1993). Voltage- and transmitter-gated currents of all-amacrine cells in a slice preparation of the rat retina. J. Neurosci. *13*, 2874–2888.

Deans, M.R., Gibson, J.R., Sellitto, C., Connors, B.W., and Paul, D.L. (2001). Synchronous activity of inhibitory networks in neocortex requires electrical synapses containing connexin36. Neuron *31*, 477–485.

Deans, M.R., Volgyi, B., Goodenough, D.A., Bloomfield, S.A., and Paul, D.L. (2002). Connexin36 is essential for transmission of rod-mediated visual signals in the mammalian retina. Neuron *36*, 703–712.

Dunn, F.A., Doan, T., Sampath, A.P., and Rieke, F. (2006). Controlling the gain of rod-mediated signals in the Mammalian retina. J. Neurosci. *26*, 3959–3970.

Euler, T., Detwiler, P.B., and Denk, W. (2002). Directionally selective calcium signals in dendrites of starburst amacrine cells. Nature *418*, 845–852.

Field, G.D., Greschner, M., Gauthier, J.L., Rangel, C., Shlens, J., Sher, A., Marshak, D.W., Litke, A.M., and Chichilnisky, E.J. (2009). High-sensitivity rod photoreceptor input to the blue-yellow color opponent pathway in macaque retina. Nat. Neurosci. *12*, 1159–1164.

Gong, S., Zheng, C., Doughty, M.L., Losos, K., Didkovsky, N., Schambra, U.B., Nowak, N.J., Joyner, A., Leblanc, G., Hatten, M.E., and Heintz, N. (2003). A gene expression atlas of the central nervous system based on bacterial artificial chromosomes. Nature *425*, 917–925.

Grimes, W.N., Zhang, J., Graydon, C.W., Kachar, B., and Diamond, J.S. (2010). Retinal parallel processors: more than 100 independent microcircuits operate within a single interneuron. Neuron *65*, 873–885.

Habermann, C.J., O'Brien, B.J., Wassle, H., and Protti, D.A. (2003). AII amacrine cells express L-type calcium channels at their output synapses. J. Neurosci. *23*, 6904–6913.

Hines, M.L., and Carnevale, N.T. (1997). The NEURON simulation environment. Neural Comput. *9*, 1179–1209.

Izhikevich, E.M. (2007). Dynamical systems in neuroscience: the geometry of excitability and bursting (Cambridge, MA: MIT Press).

Jeon, C.J., Strettoi, E., and Masland, R.H. (1998). The major cell populations of the mouse retina. J. Neurosci. *18*, 8936–8946.

Kotani, S., Hirasawa, T., Suzuki, T., Sato, K., Sakakibara, M., and Tokimasa, T. (2000). Mechanisms underlying the M-current block by barium in bullfrog sympathetic neurons. Neurosci. Lett. *285*, 1–4.

Manookin, M.B., Beaudoin, D.L., Ernst, Z.R., Flagel, L.J., and Demb, J.B. (2008). Disinhibition combines with excitation to extend the operating range of the OFF visual pathway in daylight. J. Neurosci. *28*, 4136–4150.

Münch, T.A., da Silveira, R.A., Siegert, S., Viney, T.J., Awatramani, G.B., and Roska, B. (2009). Approach sensitivity in the retina processed by a multifunctional neural circuit. Nat. Neurosci. *12*, 1308–1316.

Murphy, G.J., and Rieke, F. (2006). Network variability limits stimulus-evoked spike timing precision in retinal ganglion cells. Neuron *52*, 511–524.

Murphy, G.J., and Rieke, F. (2008). Signals and noise in an inhibitory interneuron diverge to control activity in nearby retinal ganglion cells. Nat. Neurosci. *11*, 318–326.

Oesch, N., Euler, T., and Taylor, W.R. (2005). Direction-selective dendritic action potentials in rabbit retina. Neuron *47*, 739–750.

Pang, J.J., Gao, F., and Wu, S.M. (2004). Light-evoked current responses in rod bipolar cells, cone depolarizing bipolar cells and AII amacrine cells in dark-adapted mouse retina. J. Physiol. *558*, 897–912.

Robbins, J., Trouslard, J., Marsh, S.J., and Brown, D.A. (1992). Kinetic and pharmacological properties of the M-current in rodent neuroblastoma x glioma hybrid cells. J. Physiol. *451*, 159–185.

Schnee, M.E., and Brown, B.S. (1998). Selectivity of linopirdine (DuP 996), a neurotransmitter release enhancer, in blocking voltage-dependent and calcium-activated potassium currents in hippocampal neurons. J. Pharmacol. Exp. Ther. *286*, 709–717.

Scott, L.L., Hage, T.A., and Golding, N.L. (2007). Weak action potential backpropagation is associated with high-frequency axonal firing capability in principal neurons of the gerbil medial superior olive. J. Physiol. *583*, 647–661.

Siegert, S., Scherf, B.G., Del Punta, K., Didkovsky, N., Heintz, N., and Roska, B. (2009). Genetic address book for retinal cell types. Nat. Neurosci. *12*, 1197–1204.

Strettoi, E., and Masland, R.H. (1996). The number of unidentified amacrine cells in the mammalian retina. Proc. Natl. Acad. Sci. USA *93*, 14906–14911.

Strettoi, E., Raviola, E., and Dacheux, R.F. (1992). Synaptic connections of the narrow-field, bistratified rod amacrine cell (AII) in the rabbit retina. J. Comp. Neurol. *325*, 152–168.

Tamalu, F., and Watanabe, S. (2007). Glutamatergic input is coded by spike frequency at the soma and proximal dendrite of AII amacrine cells in the mouse retina. Eur. J. Neurosci. *25*, 3243–3252.

Tian, M., Jarsky, T., Murphy, G.J., Rieke, F., and Singer, J.H. (2010). Voltage-gated Na channels in AII amacrine cells accelerate scotopic light responses mediated by the rod bipolar cell pathway. J. Neurosci. *30*, 4650–4659.

Tsukamoto, Y., Morigiwa, K., Ueda, M., and Sterling, P. (2001). Microcircuits for night vision in mouse retina. J. Neurosci. *21*, 8616–8623.

Van Wart, A., Boiko, T., Trimmer, J.S., and Matthews, G. (2005). Novel clustering of sodium channel Na(v)1.1 with ankyrin-G and neurofascin at discrete sites in the inner plexiform layer of the retina. Mol. Cell. Neurosci. *28*, 661–673.

Vardi, N., and Smith, R.G. (1996). The AII amacrine network: coupling can increase correlated activity. Vision Res. *36*, 3743–3757.

Veruki, M.L., and Hartveit, E. (2002a). AII (Rod) amacrine cells form a network of electrically coupled interneurons in the mammalian retina. Neuron *33*, 935–946.

Veruki, M.L., and Hartveit, E. (2002b). Electrical synapses mediate signal transmission in the rod pathway of the mammalian retina. J. Neurosci. *22*, 10558–10566.

Veruki, M.L., Oltedal, L., and Hartveit, E. (2008). Electrical synapses between AII amacrine cells: dynamic range and functional consequences of variation in junctional conductance. J. Neurophysiol. *100*, 3305–3322.

Veruki, M.L., Oltedal, L., and Hartveit, E. (2010). Electrical coupling and passive membrane properties of AII amacrine cells. J. Neurophysiol. *103*, 1456–1466.

Völgyi, B., Deans, M.R., Paul, D.L., and Bloomfield, S.A. (2004). Convergence and segregation of the multiple rod pathways in mammalian retina. J. Neurosci. *24*, 11182–11192.

Wang, H.S., Pan, Z., Shi, W., Brown, B.S., Wymore, R.S., Cohen, I.S., Dixon, J.E., and McKinnon, D. (1998). KCNQ2 and KCNQ3 potassium channel subunits: molecular correlates of the M-channel. Science *282*, 1890–1893.

Wu, C., Ivanova, E., Cui, J., Lu, Q., and Pan, Z.H. (2011). Action potential generation at an axon initial segment-like process in the axonless retinal AII amacrine cell. J. Neurosci. *31*, 14654–14659.

Zaczek, R., Chorvat, R.J., Saye, J.A., Pierdomenico, M.E., Maciag, C.M., Logue, A.R., Fisher, B.N., Rominger, D.H., and Earl, R.A. (1998). Two new potent neurotransmitter release enhancers, 10,10-bis(4-pyridinylmethyl)-9(10H)-anthracenone and 10,10-bis(2-fluoro-4-pyridinylmethyl)-9(10H)-anthracenone: comparison to linopirdine. J. Pharmacol. Exp. Ther. *285*, 724–730.